The Whistler Traveling Wave Parametric Amplifier Driven by an Ion-Ring Beam Distribution from a Neutral Gas Injection in Space Plasmas

Paul A. Bernhardt, *Fellow, IEEE*

***Abstract*— A new parametric amplifier model describes the observations of intensified whistler waves produced by a dedicated burn of the BT-4 engine on the Cygnus spacecraft during the NG-13 mission. Ground very low frequency (VLF) radio emissions at 25.2 kHz from a Navy NML transmitter in North Dakota were amplified by 20–30 dB during the Cygnus burn at 480-km altitude and recorded at 1060 km by the e-POP/RRI plasma wave receiver on the SWARM-E satellite. The amplification process starts with charge exchange between the exhaust molecules and the ambient O+ in the ionosphere to produce water vapor ions that spiral around the earth's magnetic field lines. This ion-velocity-ring distribution generates broadband, oblique-lower-hybrid (OLH) waves, which act as a pump for the parametric amplifier. The nonlinear ponderomotive force on the electrons causes the high-amplitude OLH pump to mix with the input whistler signal, yielding an OLH idler wave. Resonant mixing of the pump and idler electric fields promotes temporal growth in the amplitude of the whistler waves as they propagate through the exhaust cloud. The key features to rocket exhaust-driven amplification (REDA) process are broadband gain, bi-directionality along the magnetic field, pump depletion, phasing, and feedback. Pump depletion limits the intensity of the output whistler waves by wave energy conservation. The total wave energy is the electrostatic energy of the pump and idler lower hybrid waves plus the energy extracted by the propagating whistler signal. The whistler traveling wave parametric amplifier provides an efficient mechanism for active amplification of signals in space.**

***Index Terms*— Active space experiments, parametric amplifier, wave–particle interactions, whistler waves.**

I. Introduction

THE natural and artificial production of high-intensity whistler waves in space is of interest because of their interaction with radiation belt particles. Lighting bursts excite large-amplitude pulses of electromagnetic (EM) radiation that couple through the bottom of the ionosphere, are ducted along magnetic field lines, and interact with the earth's radiation belts to produce lightning-induced electron precipitation (LEP). In this interaction process, amplified whistlers, triggered emissions, and enhancements in the electron density of the lower ionosphere have been observed. Similarly, ground very low frequency (VLF) transmissions from terrestrial power lines and high-power Navy communications systems have also interacted with energetic electrons found in the earth's magnetosphere. Several man-made facilities have been developed to study this wave–particle interaction (WPI) process including dedicated VLF transmitters, high-power HF facilities for modulations of natural ionosphere currents in the ionosphere, large satellite antennas driven by high-power signal generators, electron beams that are modulated at VLF rates, and high-speed neutral injections that rapidly photoionize in sunlight. All of these techniques require dedicated, expensive engineering efforts for design, construction, and testing before they are deployed on the ground or in space.

The rocket exhaust-driven amplification (REDA) technique described here uses existing technologies to amplify signals from existing ground transmitters with currently available rocket motors in low-earth-orbit. The technique converts the ambient atomic oxygen ions in the topside ionosphere to an activated plasma region with pickup ions gyrating around the magnetic field lines. Whistler waves passing though this region are parametrically amplified by converting the energy of the gyrating ions into intense EM signals. This process has been demonstrated by measurements with the e-POP/RRI instrument on SWARM-E using a dedicated burn of the BT-4 engine from Cygnus on May 26, 2020, during the NG-13 Mission [1]. During this experiment, amplifications between 20 and 30 dB of the 25.2-kHz signal from the Navy NML transmitter in North Dakota were recorded (Fig. 1). An ELF signal at 300 Hz was also amplified by more than 50 dB during the burn [1]. These two frequencies are examined with the REDA theory.

This article presents a model for a whistler traveling wave parametric amplifier (TWPA) (WTWPA) that can explain the observed intensification of the VLF waves. Whistler wave production has been previously discussed in terms of conversion from lower hybrid (LH) waves instead of amplification, as is the focus of this article. One basic mechanism for generation of whistler waves from ring-beam-driven LH waves is mode conversion on electron density striations. Eliasson and Papadopoulos [2] and Camporeale *et al.* [3] studied the linear conversion process with field-aligned irregularities (FAIs). The formation of FAIs by the ion-ring instability would be necessary for this process to be important for the REDA. In addition, the mode conversion process does not have the wave feedback needed to provide amplification of an existing whistler signal.

Manuscript received January 9, 2021; revised March 14, 2021; accepted April 27, 2021. Date of current version June 10, 2021. The review of this article was arranged by Senior Editor S. T. Lai.

The author is with the Division of Plasma Physics, US Naval Research Laboratory, Washington, DC 20375 USA (e-mail: paul.bernhardt@nrl.navy.mil).

Color versions of one or more figures in this article are available at https://doi.org/10.1109/TPS.2021.3079130.

Digital Object Identifier 10.1109/TPS.2021.3079130

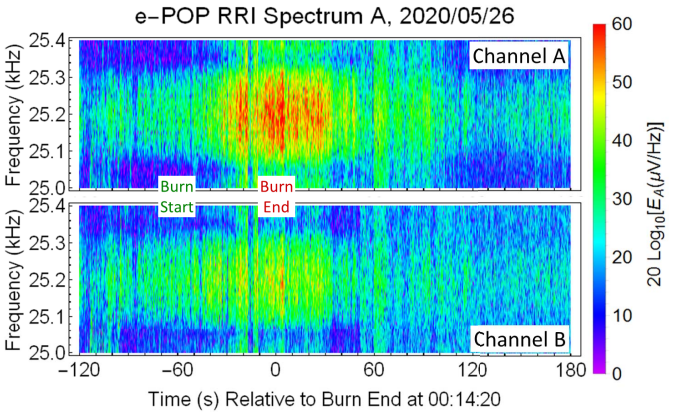

Fig. 1. Between 20- and 30-dB amplification of the 25.2-kHz ground transmissions from the NML VLF station directly below Cygnus orbiting at 500-km altitude. The radio receiver instrument (RRI) recorded the enhanced VLF signals on crossed-dipole antennas A and B at 1000-km altitude. The SWARM-E/e-POP satellite made the observations within the whistler propagation cone around the magnetic field relative to the Cygnus exhaust cloud. The measured potential on the 6-m booms comprising the RRI antennas can be converted in low-frequency electric fields with division by the boom sample distance of 3 m. The differences in the signal strengths on the two dipole-antenna channels are attributed to orientation of the dipoles and to different saturations of the input amplifiers [1].

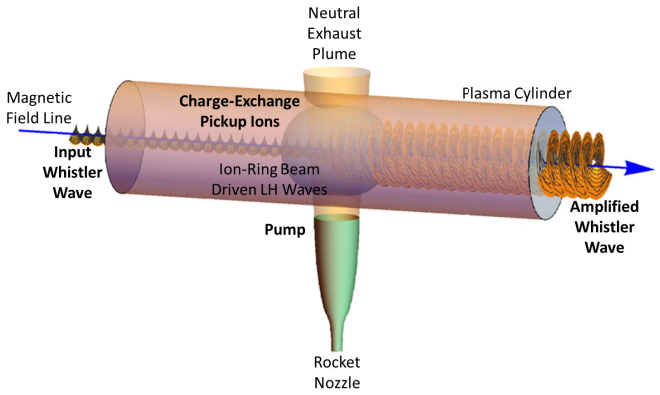

Fig. 2. Prototype design of the REDA physical device. The amplitude of the right-hand circular polarization is represented as a spiral with growth after passing though the activated region with the ion-ring beam distribution.

Parametric decay processes to *generate* whistlers with different pump waves have been proposed and studied by many authors including: 1) LH decaying to whistler and LH [4]; 2) LH decay to whistler and ion cyclotron (IC) [5]; 3) decay of IA to whistler and IA [6]; 4) parametric EM wave pumping [7]; and 5) an antenna driving two electrostatic waves with frequencies above and below the LH frequency [8]. These works have not considered *amplification* of existing waves.

To amplify whistlers, a generic WTWPA can be based on a parametric conversion process by which an electrostatic pump wave decays into a whistler wave and another daughter electrostatic wave. The parametric decay process translates into a parametric amplification process by the nonlinear ponderomotive interactions between the two oblique electrostatic waves (pump and idler) that mix to form oscillating currents to drive a parallel whistler wave. The electrostatic pump mixes with the whistler to sustain the idler wave. The dispersion relation associated with this process can be treated as an absolute instability to generate whistlers at a fixed location or it can be considered a convective instability with a complex spatial wavenumber that has an amplifying solution for propagation through the device. The kinematics of this type of propagating system was introduced by Sturrock [9].

The parametric conversion of beam-driven LH waves into whistler waves is a prime candidate for whistler parametric amplification. The electrostatic pump wave is generated by ion-ring beams from charge exchange of neutral exhaust with ambient ions in the ionosphere. Depending on the orientation of the rocket nozzle producing the supersonic neutral plume, a fraction of the charge-exchange beam will be directed along the magnetic field lines and a fraction will form a ring-beam distribution for ions gyrating around the magnetic field (B). The field-aligned ion beam will excite ion acoustic (IA) waves [10] and the perpendicular ion beam will generate LH waves [11]. Whistler waves may be generated during the growth and saturation of LH waves excited by the ring velocity distribution [12]. With a 3-D EM simulation, they employ the LH wave driven by the ion-ring distribution to model: 1) the interaction coupling of two opposite oblique LH waves into a whistler wave or 2) the decay of an oblique LH wave into a perpendicular LH wave and a parallel whistler wave. An arbitrary pump LH wave can undergo parametric decay into a daughter LH wave and the desired parallel whistler wave [4].

This article shows that an ion-ring-driven LH wave can satisfy the required matching conditions to excite parametrically a daughter LH and oblique whistler in the same non-Maxwellian plasma environment. The discussion focuses on a convective rather than absolute instability under identical conditions. The goal is to recast a parametric conversion process into a parametric amplification process by reinterpretation of the nonlinear dispersion relation of the WTWPA system.

II. Rocket Exhaust-Driven Amplification Concept

An engineering model of the REDA is illustrated in Fig. 2. The rocket nozzle injects molecules that rapidly charge exchange with the atomic ions in the plasma cylinder. These ions acquire the speed of the neutral gas but are restricted by the Lorentz force gyrate around the background lines of magnetic field. Energy from the gyrating ions is transferred to the whistler wave causing amplification.

Several processes could transfer energy from the ion motion to the EM waves. LH waves are easily excited by the gyrating ions by an ion-ring instability [12]. Electrostatic LH waves primarily propagate perpendicular to the magnetic field. Those with a finite, but small wave vector component along the magnetic field can excite whistler waves by mode conversion along field-aligned density striations [13]. This process employs FAIs that require additional energy for their production. There was no evidence of FAIs during the NG-13 experiment. The theory of parametric instabilities in the LH frequency region has been formulated using the drift kinetic equation for both fluid and kinetic regimes. The kinetic approach has studied invoking nonlinear Landau damping [14]–[16].

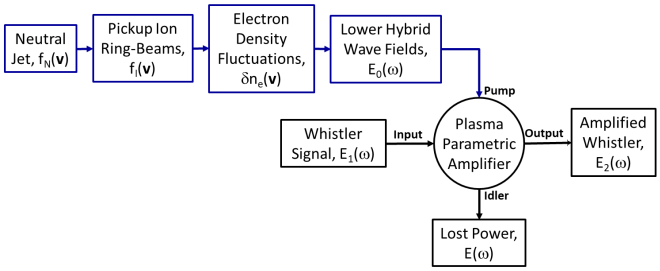

Fig. 3. Model of whistler wave amplification by neutral injections from rocket burns in space. The highlighted blue portion provides LH wave generation. The black heighted block shows the amplification portion of the theory.

A process that does not require FAIs or nonlinear wave scattering is parametric decay of the oblique, finite k_z, LH waves to a whistler plus an additional LH waves to satisfy matching conditions [4]. This process will be the basis for parametric amplification of parallel and oblique whistlers with an LH wave pump and does not require field aligned irregularities.

A block diagram of the REDA process is illustrated in Fig. 3. For the excitation of LH waves by a high-speed jet of rocket exhaust, the kinetic distribution of neutrals is converted into an ion-ring beam distribution by ion-molecular charge exchange. The energetic chemistry for supersonic exhaust production involves burning nitrogen tetroxide and hydrazine fuel to produce molecules of nitrogen and water vapor moving at 3.2 km/s from the nozzle of the rocket motor. In the upper atmosphere, these molecules react with the ambient atomic oxygen ion, yielding supersonic ions of water vapor and nitric oxide. A simplified set of exothermic reactions for this process is

$$\begin{aligned}
&N_2O_4 + 2N_2H_4 \rightarrow 4H_2O^* + 3N_2^* + 10.9\ \text{eV} \quad k_{N_2O_4-N_2H_4} \\
&\quad = 10^{-14}\text{cm}^3 s^{-1} \\
&H_2O^* + O^+ \rightarrow H_2O^{+*} + O + 1.10\ \text{eV}, \quad k_{O^+-H_2O} \\
&\quad = 3.2 \times 10^{-9}\text{cm}^3 s^{-1} \\
&N_2^* + O^+ \rightarrow NO^{+*} + N + 1.10\ \text{eV} \quad k_{O^+-N_2} \\
&\quad = 1.1 \times 10^{-12}\text{cm}^3 s^{-1}. \qquad (1)
\end{aligned}$$

Neglecting transport, the density of activated ion rings, n_r, is estimated with a steady-state solution of the rate equation

$$\begin{aligned}
\frac{\partial n_r}{\partial t} &= k_{\text{CE}} n_{H_2o} n_{O^+} - k_{\text{DR}} n_r n_{e^-} = 0, \quad n_{e^-} = n_r + n_{O^+}, \ n_r \\
&= \frac{k_{\text{CE}} n_{e^-} n_{H_2o}}{k_{\text{DR}} n_{e^-} + k_{\text{CE}} n_{H_2o}} \qquad (2)
\end{aligned}$$

where the values for the charge exchange rate $k_{\text{CE}} = 3.2 \times 10^{-9}$ cm^3/s from (1) and dissociative recombination rate $k_{\text{DR}} = 3.6 \times 10^{-7}$ cm^3/s [17]. The equilibrium ring-ion density is related to the conversion of neutral kinetic energy to pump LH wave energy by a constant fraction α_S given by

$$\begin{aligned}
\alpha_C &= \frac{n_r}{n_{H_2O}} = \frac{k_{\text{CE}} n_{e^-}}{k_{\text{DR}} n_{e^-} + k_{\text{CE}} n_{H_2o}} \\
W_{rS} &= \frac{1}{2} m_r V_r^2 \alpha_C n_{H_2O}, \quad \alpha_S = \frac{W_{0S}}{W_{rS}} \qquad (3)
\end{aligned}$$

where α_C is the charge exchange, conversion efficiency, W_{rS} is the water ion source energy, and W_{0S} is the electrostatic

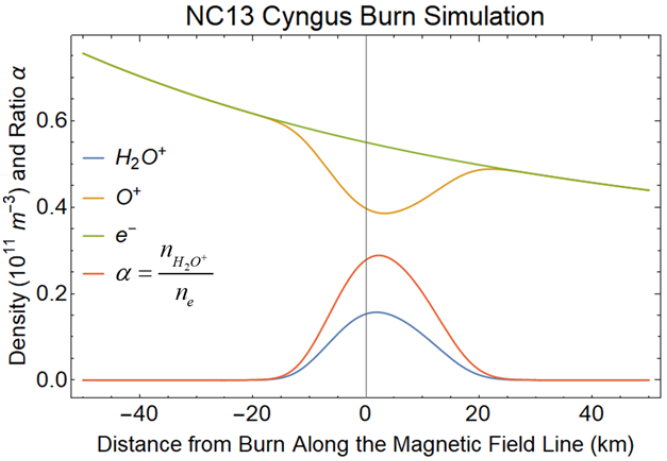

Fig. 4. Plasma densities provided by a model of the neutral jet driving the ion plasma chemistry and transport equations for the NC-13 Cygnus burn on May 26, 2020. The magnetic field line is located at the end of a 60-s burn. The time of the simulation is 1 s after the burn stops. The whistler wave is amplified as it travels from left to right along **B**, extracting energy from the H_2O+ ions at the center of the figure.

energy of the LH wave. For the NG-13 REDA experiment, $\alpha_C = 0.0088$ and $_{Wr}\text{S} = 2.45 \times 10^{-10}$ J/m3.

The fraction of activated ions $\alpha = n_r/n_e$ is a critical parameter for driving the REDA process in the plasma. This fraction is computed using the time-dependent models [1], [18], which couples the neutral expansion of the exhaust cloud with the background plasma using the chemical reactions from (1). A simulation of the NG-13 Cygnus experiment is used to generate the plasma densities illustrated in Fig. 4. This plasma profile is taken 1 s after the burn stops along the magnetic field line at the burn termination point but it is representative of the density of activated ions ~7 km behind Cygnus during the full 60 s of the burn. The ion-ring distribution for NC-13 has an activation fraction of about 30% in a region with a full width of about 25 km. Amplification occurs for whistler mode waves passing through this region by the WTWPA process.

There are three methods for the detection of the ion-ring distribution of H_2O^+ molecules. First, ground incoherent scatter radar (ISR) can measure the ion line spectra with the radar beam pointed at the exhaust cloud in the plasma. The ISR technique provided confirmation of ion-ring generation using the Arecibo ISR based on observations from ST-93 in 1999 using a burn of the Space Shuttle OMS engines [19]. The second technique is *in situ* measurements of the ion-velocity distribution on a satellite with an ion-drift meter. This technique was used on STS-127 with the Space Shuttle OMS engines injected an exhaust cloud across the trajectory of the ion-velocity meter (IVM) on the CINDI instrument package hosted by the AFRL C/NOFS spacecraft. The presence of the artificial fast ions was detected by both ion plasma drift and composition measurements [20]. The third technique is observations of residual plasma hole in the ionosphere after the molecular ions in the ring distribution have recombined with ambient electrons [20], [21]. The GPS TEC measurements from the GAP instrument on e-POP/SWARM-E clearly show a density depression 200 s after the end of the Cygnus burn of NT-13 (Fig. 5).

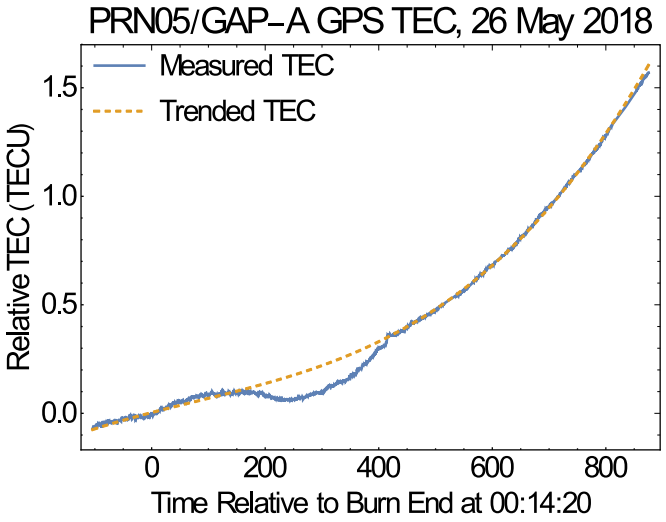

Fig. 5. Plasma depression attributed to recombination of water ions in the ion-ring-velocity distribution of that drives the whistler parametric amplifier. The time variation is the TEC measurement occurs as the satellite in low-earth-orbit records signals along a path that transits the disturbed region of the ionosphere.

In conclusion, it has been firmly established that a rocket motor injecting neutral molecules across magnetic field lines in the ionosphere will create an ion-ring distribution. The generation of LH waves is the next step in the REDA process and will be explored in the following section.

A. Lower Hybrid Wave Generation

The LH pump waves are easily generated in a low-beta plasma by an ion-velocity ring distribution. Modeling of this process requires both linear theory for wave growth and kinetic simulations in two or three spatial dimensions [11], [12]. The plasma velocity distributions in the model are given for the ambient electrons, background ions, cold ring-beam ions, and warm ring-beam ions, respectively, as

$$
\begin{aligned}
f_e^b(\mathbf{v}) &= \frac{1}{\pi^{3/2} v_e^3} \exp\left(-\frac{v^2}{v_e^2}\right) \\
f_i^b(v_\perp, v_\parallel) &= \frac{1}{\pi^{3/2} v_{i\perp}^2 v_{i\parallel}} \exp\left(-\frac{v_\perp^2}{v_{i\perp}^2} - \frac{v_\parallel^2}{v_{i\parallel}^2}\right) \\
f_i^r(v_\perp, v_\parallel) &= \frac{1}{2\pi u_{m\perp}} \delta(v_\perp - V_r)\delta(v_\parallel - V_z) \\
f_i^r(v_\perp, v_\parallel) &= \frac{1}{\left(2\pi v_m^2\right)^{3/2}} \exp\left[-\frac{\left(v_\parallel - V_z\right)^2 + v_\perp^2 + V_r^2}{2v_m^2}\right] \\
&\quad \times I_0\left(\frac{v_\perp V_r}{v_m^2}\right). \qquad (4)
\end{aligned}
$$

Representative experimental parameters for these distributions are given as electron thermal speed $v_e \approx 100$ km/s, ion perpendicular and parallel thermal speed $v_{i\perp} \approx v_{i\perp} \approx 1$ km/s, ion-ring velocity $V_r \approx 4$ km/s, ion beam parallel velocity $V_z \approx 1$ km/s, and ion-ring beam thermal speed $v_m \approx 0.1$ km/s for a retrograde (i.e., wake) Cygnus engine burn that subtracts the exhaust speed from the satellite orbit motion [1].

The plasma velocity distributions shown in Fig. 6 illustrate a broad velocity space spectrum of electrons (orange), a warm

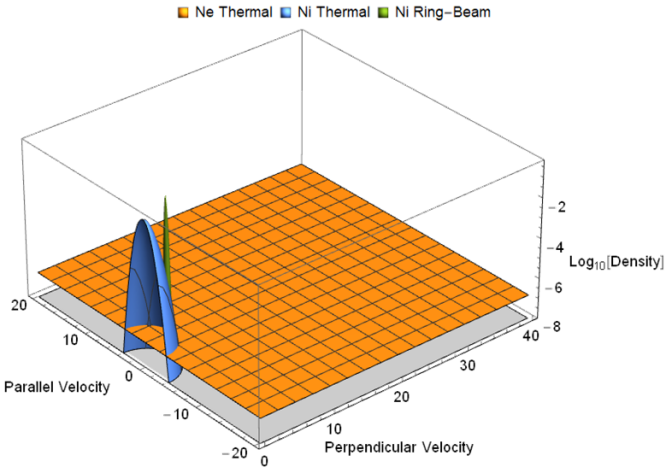

Fig. 6. Representative velocity distributions for the REDA experiment conducted during the NG-13 Cygnus mission.

spectrum of background ions (blue), and a cold spectrum of pickup ions (green) produced from the cold but swift neutral atoms from the rocket motor. These kinetic distribution functions are used to derive the electrostatic linear dispersion equation for LH waves driven by the ring distribution [22]. Because rocket exhaust and created pickup ions are cold, the dispersion equation for the LH waves is derived using the third (rather than fourth) ring distribution function in (4).

The electrostatic wave dispersion function can be derived from fluid theory using Poisson's equation, the linearized equations of motion, and the equations of continuity for the electrons and ions [4]. For the ion-ring distribution, the generalized dispersion formulation [11], [22] employs the following integrations for relating pump density n_{0i} and electric potential ϕ_{0i} oscillations

$$
\begin{aligned}
\frac{e}{\varepsilon_0} n_{0i} = \phi_{0i}\omega_{\mathrm{pi}}^2 \int_{-\infty}^{0} dt e^{-i\omega t} \int_0^\infty v_\perp dv_\perp \int_0^\infty dv_{||} \\
\times \int_0^{2\pi} d\theta \exp(i\mathbf{k}_0 \cdot \mathbf{v}t)\mathbf{k}_0 \cdot \nabla_{\mathbf{v}} f. \qquad (5)
\end{aligned}
$$

Substitution of the first three distributions of (4) in Poisson's equation yield the LH dispersion

$$
\begin{aligned}
D_{\mathrm{LH}}^{\mathrm{ES}}(\omega_0, \alpha) = 1 + \frac{\omega_{\mathrm{pe}}^2}{\omega_{\mathrm{ce}}^2} - \frac{\omega_{\mathrm{pe}}^2 k_{0z}^2}{\omega_0^2 k_0^2} - (1-\alpha)\frac{\omega_{\mathrm{pi}}^2}{\omega_0^2} \\
- \frac{\alpha\omega_{\mathrm{pi}}^2 \omega_0 m_i/m_r}{\left(\omega_0^2 - k_{0x}^2 V_r^2\right)^{3/2}} = 0 \qquad (6)
\end{aligned}
$$

where α is the fraction of total ions in a velocity ring, V_r is the perpendicular ion speed, m_r and m_i are the respective ring and background ion masses, ω_0 is the LH frequency for the pump wave, $k_{0x} = k_0 \sin\theta_0$ is the perpendicular wavenumber, $k_{0z} = k_0 \cos\theta_0$ is the parallel wavenumber, θ_0 is the wave vector angle with magnetic vector $\mathbf{B}$, and $\omega_i^2 = n_i e^2/(m_i \varepsilon_0)$, $\omega_e^2 = n_{e0} e^2/(m_e \varepsilon_0)$, and $\omega_{\mathrm{ce}} = eB/m_e$ are the ion–plasma, electron–plasma, and electron–cyclotron frequencies, respectively. The warm ring-beam distribution is not used because the rocket exhaust is produced from the nozzle with an extremely cold temperature of about 120 K or 0.01 eV [20] relative to

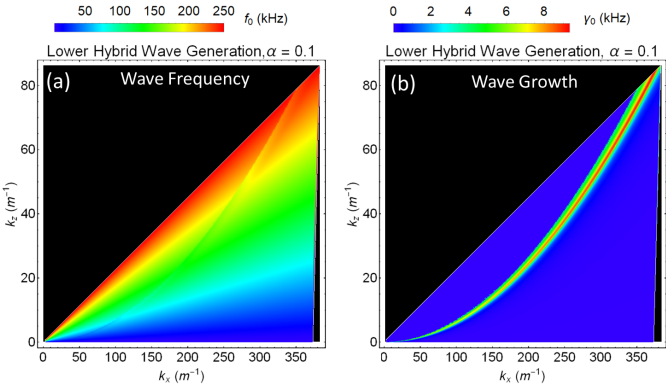

Fig. 7. Numerical solutions of the LH wave dispersion equation with 10% of the ions in a ring velocity distribution. Maximum LH instability growth is found for propagation nearly perpendicular to **B**.

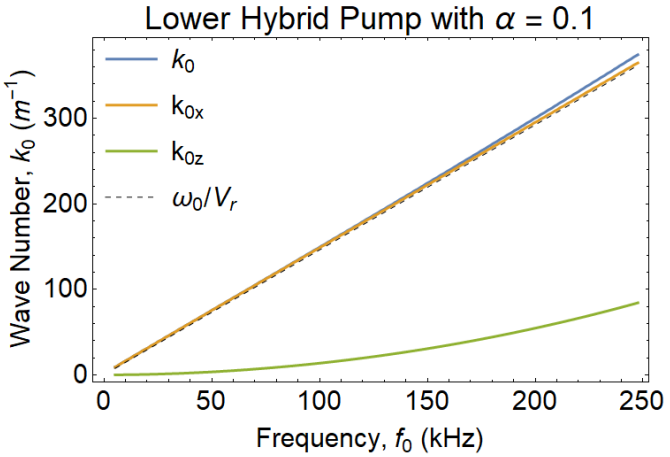

Fig. 8. Computed wavenumber dispersions of the largest growing LH waves that are the free energy sources for the WTWPA.

the neutral injection speed at 4 km/s with 1.5-eV energy. After charge exchange, the ions are produced with the same low temperature, so the ion-ring-beam distribution is definitely not warm. For this reason, the cold plasma is justified and a warm ion distribution in (6) is not considered.

Numerical solutions of (6) give the LH wave frequency ω_0, growth rates γ_0 of the LH wave instability for a range of wave numbers k_0 and wave propagation angles θ_0 [Fig. 7(a) and 7(b)]. Away from cyclotron resonance, the wave growth vanishes and the LH wave dispersion is for a Maxwellian plasma composed of background and pick ion masses m_i and m_r, respectively. At the cyclotron resonance region, the LH wave eigenvalues for resonant frequency and growth rate change significantly.

For each LH wave propagation direction, the numerical values of perpendicular wavenumber (Fig. 8) are found to be consistent with the approximations to the cyclotron resonance formulas [12]

$$\omega_0 \approx \omega_{ce}\cos\theta_0 \quad \text{and } k_{0x} \approx \frac{\omega_0}{V_R} \approx \frac{\omega_{ce}\cos\theta_0}{V_R}. \tag{7}$$

The ion cyclotron resonance $k_{0x} = \omega_0/V_r$ closely, but not exactly, matches the computed dispersion for the LH pump wave. The following section shows that an idler wave will be produced by the whistler parametric wave amplifier that is off

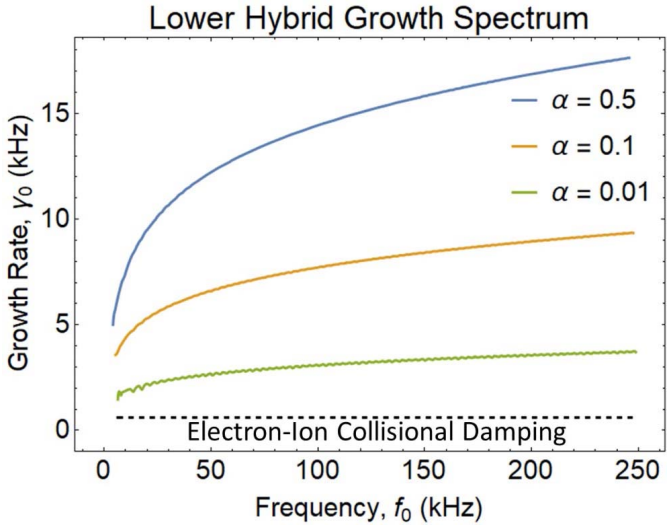

Fig. 9. Wide-frequency range of LH pump wave growth with different values of ion-ring density fraction. The instability is active over the entire spectrum because the growth rate is larger than the rate of electron–ion damping in the background plasma.

the LH resonance (6) but will follow the same dispersion as shown in Fig. 7(a).

Tracing out the LH wave frequency at the maximum growth rate gives the wavenumber dependence for the pump wave shown in Fig. 9 for a three of ion-ring densities relative to the background. The growth rate is strongly dependent on the ion-ring density fraction α in the ambient plasma. The spectrum of oblique LH waves available to support the whistler mode amplification for the NG-13 experiment is computed cover the frequency range from the local LH frequency (6.447 kHz) to over 500 kHz. The simulations in this article will use values of $\alpha = 0.1$ which is consistent with the computed ring-ion densities illustrated in Fig. 4. The evolution of the ion-velocity distribution in the plasma needs to be studied with a kinetic mode using particle ions.

The ion-ring fraction, α, effects on the properties of the plasma. First, α must be large enough to drive oblique LH wave growth above damping by collisional and wave–wave interaction losses. The LH damping rate [23], [24] is given as

$$\gamma_e = \frac{\nu_e}{2}\left(1 - \frac{\omega_{LH}^2}{\omega_0^2} + \frac{\omega_{LH}^2}{\omega_{ce}\omega_{ci}}\right) \cong \nu_e. \tag{8}$$

Second, α changes the plasma composition.

The saturation amplitudes and time histories of the LH waves cannot be obtained using linear theory. Kinetic particle in cell (PIC) and hybrid (particle ions and fluid electron) codes permit running the models to equilibrium for estimation of the pump electric field amplitudes as a function of input kinetic energy from the pickup ions. These types of simulations have been reported for both EM and electrostatic fields with ion-ring velocity distributions as drivers [12], [25]–[27]. The energy density is computed assuming that the LH wave potential has the form $\phi_{0S} = A_{0S}\exp[-i(\omega_0 t - k_{0x} - k_{0z}z)]$, where A_{0S} is the amplitude of the source potential. The results of a particle simulation model can provide energy density inside the fields

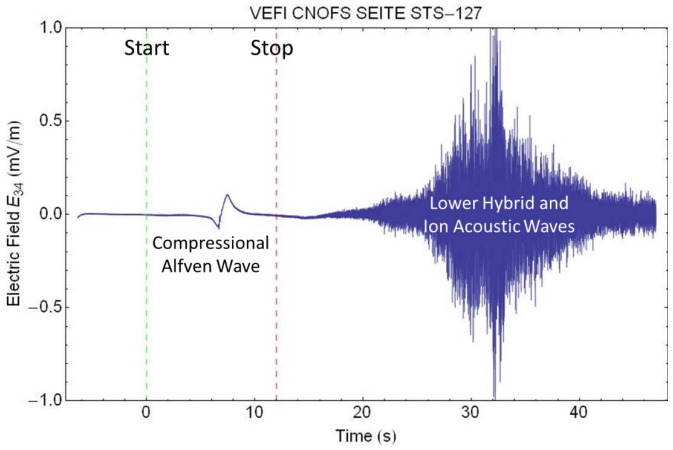

Fig. 10. MHD and electrostatic waves generated by the 12 s OMS burn on the Space Shuttle mission STS-127 on July 20, 2009. Figure adapted from [20].

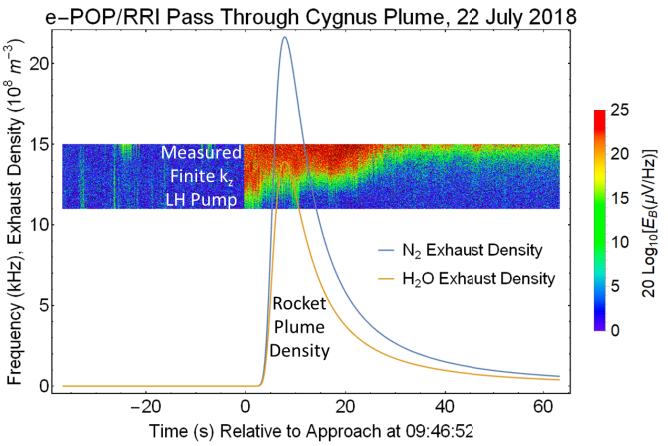

Fig. 11. Cygnus OA-9E experimental verification that neutral exhaust can produce intense LH waves a distances over 50 km from the source. The displayed data show the only enhanced VLF signals from the e-POP RRI sensor, which operated in the 0–36-kHz range. Figure adapted from [18].

with the expression [28]

$$W_{rS} = \frac{\varepsilon_0 |A_{0S}(z)|^2}{4} F_{\mathrm{ES0}}, \quad \text{where } F_{\mathrm{ES0}} = k_{x0}^2 \left(1 + \frac{\omega_{\mathrm{pi}}^2}{\omega_0^2} + \frac{\omega_{\mathrm{pe}}^2}{\omega_{\mathrm{ce}}^2}\right) + k_z^2 \left(\frac{\omega_{\mathrm{pe}}^2}{\omega_0^2}\right). \tag{9}$$

This is then inserted into (3) to give the conversion efficiency from the neutral gas kinetic input to the REDA. For now, we will only investigate the REDA process as a function of driving LH wave potential, not as a function of the rocket motor neutral density flux.

Experimentally, the generation of broadband LH waves with rocket exhaust has be verified by flying an electric field receiver though neutral gas plume in the topside ionosphere. Measurements of enhanced low-frequency electrostatic waves have been excited by rocket engine exhaust [20]. Dedicated burns of the orbital maneuver subsystem (OMS) engines on the Space Shuttle were performed during the STS-127 and STS-129 missions in 2009 to produce a hypersonic exhaust cloud that intercepted the orbit of the AFRL C/NOFS satellite. Each OMS engine produced exhaust flow rate of 10 kg/s, which is 67 times larger than the Cygnus BT-4 flow rate of 0.15 kg/s.

In situ measurements by the VEFI electric field instrument showed 20-dB enhancements in electrostatic noise up to 4 kHz when the exhaust cloud passed over C/NOFS. Fig. 10 shows the *in situ* observations of the electric field oscillations from the 12-s OMS burn that traveled 87 km to the VEFI electric field instrument on C/NFOS. The first wave is a compressional Alfven or fast MHD wave produced by bulk compression of the ionosphere by the engine burn. This wave propagates at the Alfven speed from the OMS engines reaches C/NOFS before the exhaust cloud. The large-amplitude electric fields, 30 s after the start of the burn, are *in situ* electrostatic waves produced by streaming pickup ions driving ion-beam instabilities causing both LH and ion-acoustic emissions. The *in situ* CINDI probes on C/NOFS observed changes in composition, ion temperature, and ion velocity attributed to CO_2^+ ions produced by charge exchange with the supersonic spacecraft exhaust and collisional heating in the background atmosphere [20].

More recently, the impact of a rocket engine burn on the plasma wave environment was recorded on July 22, 2018, when the RRI/e-POP plasma wave receiver passed within 50 km of the Cygnus satellite on the OA-9E mission [18]. Before the burn, the RRI spectra showed a weak VLF signal at 19.8 kHz from the NWC transmitter 5000 km away in Australia, the LH cutoff for unducted whistlers near 6.8 kHz and a spacecraft-induced LH wave signal near 17 kHz. There were no emissions in the 12–15-kHz band. Twenty seconds after the start of the 30-s burn, at the time of closest approach for the satellites, a broad spectrum of LH waves is observed in the RRI spectrum. This spectrum persisted for 20 s before returning to the preburn frequency display. A comparison of the computed exhaust density and the intensity of the exhaust induced LH turbulence shows a strong correlation (Fig. 11). For the full data spectra [18], it is noted that the intensity of the 19.8-kHz VLF signals is undisturbed by the high-speed injection of neutrals, so there was no sign of whistler wave amplification during the OA-9A [18].

In summary, the rocket exhaust can excite oblique LH (OLH) waves in the frequency range of 5 kHz to over 250 kHz. The growth rate of the LH instability is primarily affected by the fraction of energetic pickup ions relative to the total ion density. Consequently, the pump-wave energy source is expected to be largest at the center of the exhaust plume where more ambient ions are converted into supersonic molecular exhaust ions. The transfer of energy from the pump to the whistler signal wave is dependent on the intensity of the rocket exhaust-driven OLH waves. As the whistler propagates into the exhaust cloud, the rate of amplification will increase and will taper off as the wave exits the cloud with a fully amplified signal. The details of the amplification process inside the cloud are considered next.

B. Whistler Mode Parametric Amplification

The parametric amplification in a uniform plasma for the decay of an LH wave into a whistler and another LH wave is used to provide spatial growth of the whistler signal. Spatial parametric amplification in a plasma is not novel. For

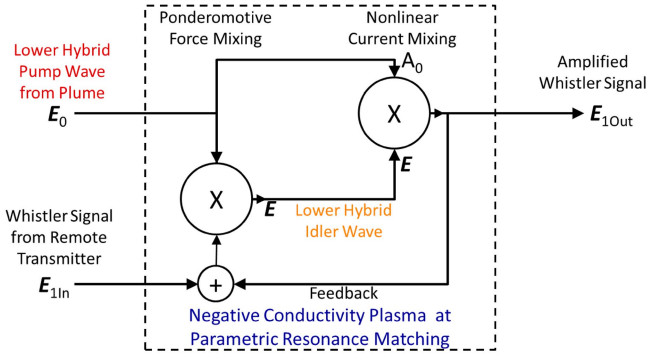

Fig. 12. Functional diagram of the whistler parametric amplifier. With an input whistler signal, mixing with the LH pump yields an LH idler that extracts energy from the pump to produce coherent amplification of the whistler. At resonance, the phase-matched feedback of the amplified signal leads to both spatial and temporal growth.

example, convective amplification by a three-wave parametric process has been investigated for the two-electron plasma (EP) waves produced by the two-plasmon decay instability for an EM wave in an inhomogeneous plasma [29], [30]. Similarly, the EM wave decay into another EM wave and an IA wave has been shown to produce convective Brillouin amplification in a drifting plasma [31] or the EM decay into an EM and EP wave produces convective Raman amplification in an inhomogeneous plasma [32]. The whistler mode parametric amplifier follows a similar process with different pump and signal waves.

A rocket burn produces the pump oblique-LH (OLH) waves required for REDA. The WTWPA comprises seven key features of temporal wave growth, spatial amplifier gain, bi-directionality, nonlinearity, feedback, phasing, and pump depletion. These features are illustrated in the functional diagram shown in Fig. 12. Without an input whistler signal, an LH pump signal $\mathbf{E}_0$ decays into a whistler wave $\mathbf{E}_{1\mathrm{Out}}$ and an LH wave $\mathbf{E}$. Since the LH turbulence produced by the rocket exhaust has a broad frequency range, the parametric decay without an input signal could yield a broad frequency range for whistler waves. A monochromatic whistler mode input $\mathbf{E}_{1\mathrm{In}}$ stimulates WTWPA to operate at only one frequency ω_0 with the decay given by the frequency matching relation $\omega_0 = \omega_1 + \omega$ for the whistler and LH idler waves, respectively. This is the distinction between a broadband generation device and a monochromatic amplification device.

Whistlers can experience temporal growth in a plasma driven by a strong LH wave. Any propagating wave passing through a medium of temporal growth also shows spatial amplification. The gain of the WTWPA depends on the strength of the LH pump and the spatial dimensions of the activated plasma region. The WTWPA is bi-directional because the amplification that occurs along the magnetic field lines is symmetric. The WTWPA employs the coupling between the pump wave at ω_0, signal wave at ω_1, and the idler wave a ω. Second-order quadratic nonlinearities occur in plasmas because of the products of density and velocity in expressions for: 1) plasma flux and current; 2) velocity and magnetic field in the expression for momentum; and 3) dual-frequency, velocity oscillations in the expression for plasma convection. The WTWPA system densities, velocities, and fields have fluctuations at the three frequencies ω_0, ω_1, and ω. Quadratic nonlinearities in the amplifier yield the sums of these frequencies.

TABLE I
PLASMA PARAMETERS IN THE NG-13 CYGNUS BURN SYSTEM

Plasma Property	Variable Name	Cygnus 480 km Altitude
Electron Plasma Frequency	f_{pe}	3.135 MHz
Ion Plasma Frequency	f_{pi}	108.47 kHz
Electron Gyro Frequency	f_{ce}	1.187 MHz
Ion Gyro Frequency	f_{ci}	41.2 Hz
Lower Hybrid Frequency	f_{LH}	6.447 kHz
Electron Collision Frequency	ν_e	607 Hz
Alfven Speed	V_A	689 km/s
Electron Thermal Speed	v_{Te}	241 km/s
Ion Acoustic Speed	v_{IA}	1.418 km/s
Ion Thermal Speed	v_{Ti}	1.372 km/s
Plasma Beta	β	4.2×10^{-6}
Cygnus Exhaust Speed	V_r	4.3 km/s
Cygnus Exhaust Spread	δV_r	0.235 km/s
Injected Ion Gyro Radius	ρ_i	104.4 m

The REDA experiment during the NG-13 Cygnus mission provides a set of parameters to test the WTWPA model. The amplification theory developed in this section will use the plasma conditions from the NG-13 Cygnus burn [1] given in Table I. The electric field strength of the amplified whistlers will be taken from the RRI measurements shown in Fig. 1. Both the 300 Hz (ELF) and 25.2 kHz (VLF) frequencies for the observed NG-13 amplifications will be used in the simulations.

A number of well-known features are embodied in the WTWPA representation of REDA. The governing relations for the parametric process of the WTWPA are provided by the Manley–Rowe relations $\omega_0 = \omega_1 + \omega$ and $\mathbf{k}_0 = \mathbf{k}_1 + \mathbf{k}$. These expressions have been applied to electronic circuits, nonlinear optics [33], and nonlinear plasmas [34], [35]. Feedback enhances the gain of a bi-directional, parametric amplifier if the active media is imbedded in a cavity. Such cavities are found with magnetic whistler ducts with reflecting endpoints where magnetic fields converge [1], [24], [36], and [37]. Proper phasing is required for positive interference between the waves to provide amplification. Finally, pump depletion limits the amount of power coming out of microwave parametric amplifiers, optical parametric amplifiers, and as well as the WTWPA described here.

The derivation of the whistler parametric amplifier follows discussions of nonlinear waves and pondoromotive force [28], [38] and the parametric conversion theory [4]. Three coupled waves in the WTWPA are represented as

$$\begin{aligned}
\text{Electrostatic LH Pump: } \phi_0 &= A_0 e^{-i(\omega_0 t - k_{0x} x - k_{0z} z)} \\
\text{Electrostatic LH Idler: } \phi &= A e^{-i(\omega t - k_x x - k_z z)} \\
\text{Electromagnetic Whister: } \mathbf{E}_1 &= A_1(\hat{x} + i\hat{y}) e^{-i(\omega_1 t - k_{1x} x - k_{1z} z)} \\
\mathbf{B}_1 &= (\mathbf{k}_1 \times \mathbf{E}_1)/\omega_1. \qquad (10)
\end{aligned}$$

The electrostatic waves given as potential amplitudes A_0 and A. The "slow" z-variations of these amplitudes along **B** are neglected because they are much smaller than the wave variations associated with wave numbers k_{0z} and k_z. Note that all quantities associated with the pump and idler waves will be denoted with subscripts 0 and "blank," respectively. The EM wave, with subscript "1," is right circularly polarized with electric-field-amplitude function A_1 and the magnetic field amplitude $-iA_1k_1/\omega_1$. The z variations of the electrostatic pump and idler waves will result from localized matching the second-order relationships to the EM wave. The whistler mode propagates at angle θ_1 relative to the magnetic field direction so $k_{1z} = k_1 \sin\theta_1$. Here, only purely longitudinal propagation is considered for the whistler wave, so θ_1 is set to zero. This theory can be extended to amplification of oblique whistlers in the future. Finally, the dispersion of the idler wave is assumed to be far enough from the ion cyclotron resonance and the only effect of the pickup ions is a change in ion mass.

Computing the parametric conversion of LH to whistler waves requires satisfying: 1) the plasma dispersion [28], [39] for the whistler signal frequency at ω_1:

$$D_1(\omega_1, k_1) = k_1^2 - \frac{\omega_1^2}{c^2} - \frac{\omega_1\omega_{\rm pe}^2}{c^2\omega_{\rm ce}\cos\theta_1} = 0 \tag{11}$$

and the idler (oblique or finite kz LH) mode at ω using (6) with $_{V_r} = 0$

$$D(\omega, k_x, k_z) = 1 + \frac{\omega_{\rm pe}^2}{\omega_{\rm ce}^2} - \frac{\omega_{\rm pe}^2 k_z^2}{\omega^2 k^2} - \left[1 - \alpha\left(1 - \frac{m_i}{m_r}\right)\right]\frac{\omega_{\rm pi}^2}{\omega^2} = 0 \tag{12}$$

2) the ion-velocity-ring instability conditions (7) for the pump wave

$$\omega_0 = \omega_{\rm ce}\frac{k_{0z}}{k_0}, k_{0x} = \frac{\omega_0}{V_r}, k_{1x} = k_1\sin\theta_1, k_{1z} = k_1\cos\theta_1 \tag{13}$$

and 3) the Manley–Rowe wave-matching conditions. Given a whistler signal frequency (ω_1) and propagation direction ($\theta_1 = 0$ or $k_{1x} = 0$), ten equations above are solved for the ten equilibrium wave parameters. The LH dispersion (12) with $k_z = 0$ provides the LH frequency of the two-ion plasma as

$$\omega_{\rm LH} = \sqrt{\frac{(1-\alpha)\omega_{\rm pi}^2 + \alpha\omega_{\rm pr}^2}{1 + \omega_{\rm pe}^2/\omega_{\rm ce}^2}}. \tag{14}$$

The ion-velocity-ring instability conditions (12) are only good for wave matching when the plasma is dominated by the pick-up ions from the rocket motor. This lasted for 60 s during the NG-13 experiment at the position of the exhaust injection. The ion-neutral collision time 500-km altitude is 283 s, which is longer than the period of observed 25.2-kHz wave amplification shown in Fig. 1. The injected neutrals produce a long-lasting ion-ring distribution that is mainly scattered in velocity space by wave–particle interactions during the burn. For this reason, (12) is well justified to prescribe the matching conditions in the model.

The wave-matching conditions (11)–(13) are used to find the frequencies, wavenumbers, and propagation angles given an incident whistler wave with frequency ω_1 and propagation angle θ_1. For a parallel whistler with $\theta_1 = 0$ and assuming that the electron gyro frequency is much larger than the pump, signal or idler frequencies, the resonating pump frequency can be found from

$$\omega^2 = (\omega_0 - \omega_1)^2 = \omega_{\rm LH}^2 + \frac{\omega_0^2\omega_{\rm pe}^2}{1 + \omega_{\rm pe}^2/\omega_{\rm ce}^2}\left(\frac{1 - \sqrt{1 + 4k_1V_R/\omega_{\rm ce}}}{k_1V_R + \omega_0^2/\omega_{\rm ce}}\right)^2. \tag{15}$$

The largest real root for ω_0o of (15) is approximately $\omega_1 + \omega_{\rm LH}$. The close relationship between the LH idler frequency w and the LH frequency $\omega_{\rm LH}$ is presented in Fig. 13 for the parameters of Table I, showing that the difference between those frequencies is only –25 Hz. The WTWPA process works over the full range of whistler signal frequencies if there is sufficient pump wave energy available at each ω_0o that satisfies the matching conditions.

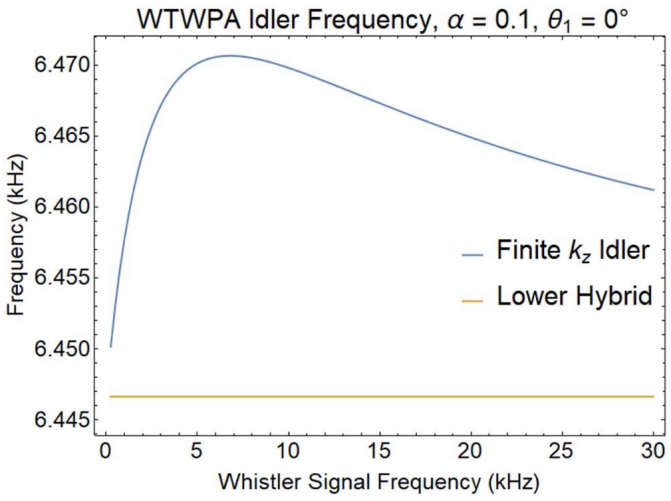

Fig. 13. The idler wave frequency compared to LH frequency of 6.447 kHz. The idler is a finite k_z LH wave that is produced as a mixing product in the WTWPA. The mixing occurs between parallel propagating whistler waves and the rocket exhaust-driven pump wave, which has finite k_z.

An example of the wave-matching conditions for both frequency and wavenumber of a 300 Hz signal is shown in Fig. 14. The wave matching is examined for a whistler propagating into the cloud of activated LH waves. The amplified ELF signal during NG-13 at $f_1 = 300$ Hz satisfies the pump wave-matching equations that are illustrated in Fig. 14 for $\alpha = 0.1$. The pump (red) and idler (orange) LH waves combine to give the whistler (black) with the wave and frequency matching at the top of the figure along with satisfying the dispersion equations (11) and (12). The pump wave at 6.75 kHz, when driven by the BT-4 exhaust from Cygnus resonates, has an LH growth rate of 1.82 kHz according to the theory of Section A. This is greater than the collisional frequency of 607 Hz, so the LH pump has sufficient free energy to drive the WPA through wave kinetic processes. The daughter LH wave has a frequency of 6.45 kHz. Both LH waves propagate at an angle almost perpendicular to **B** near 89.7°. The small difference in the LH wave propagation angles is enough to support the small EM wave vector along **B** for the whistler mode signal.

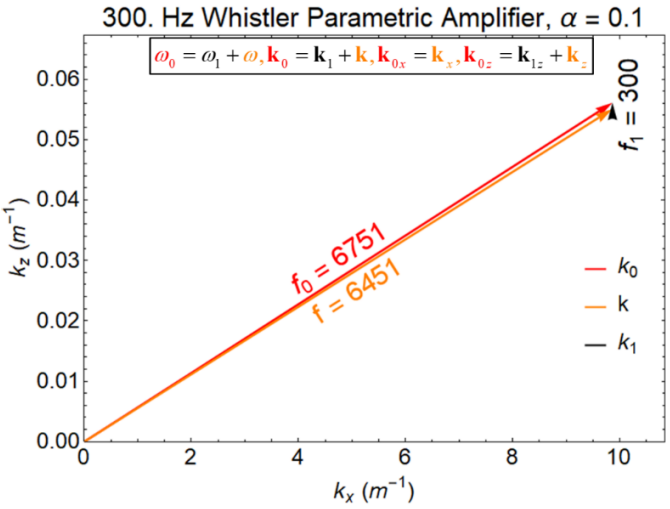

Fig. 14. Pump and idler wave parameters for exciting a 300-Hz parametric amplifier with the whistler wave entering the exhaust ion cloud ($\alpha = 0.1$) and with the background plasma and neutral injection specified in Table I. The growth rate of the 6.75-kHz pump wave is $\gamma_0 = 1.82$ kHz when driven by the 4.3 km/s ion-ring distribution.

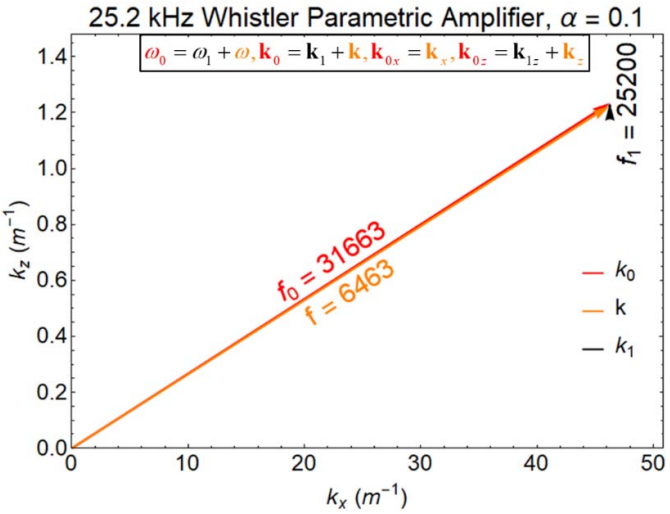

Fig. 15. Pump and idler wave parameters for exciting a 25.2-kHz whistler parametric amplifier with the same neutral injection as Fig. 14. The growth rate of the 31.66-kHz pump wave is $\gamma_0 = 2.39$ kHz when driven by the 4.3 km/s exhaust cloud.

The matching conditions work equally well, with signal frequency is elevated into the VLF band at $f_1 = 25.2$ kHz for the $\alpha = 0.1$ pump of Fig. 7. The resulting wave-matching diagram is shown in Fig. 15. In this case, the pump-wave growth rate is 2.39 kHz, which is again much larger than the ambient electron collision frequency. For the REDA, the ambient plasma density must be large for sufficient charge exchange with the injected exhaust but the ambient neutral density must be low to prevent collisional damping of the low hybrid instability that drives the pump wave. The topside region of the ionosphere satisfies this requirement. Table I with Figs. 14 and 15 provide sample sets of resonant parameters with which to test the REDA theory.

The resonant whistler parametric amplifier is described by two coupled nonlinear wave equations, one for the whistler signal and one for the finite-k_z, OLH idler. The analysis starts with the parametric decay of the pump OLH wave into whistler signal and OLH idler waves.

The whistler signal wave is derived from Maxwell's curl equations with currents provided by the wave electric field and the product of electron density perturbations and velocity oscillations at different frequencies [4] result in

$$\begin{aligned}\nabla^2\mathbf{E}_1 - \nabla(\nabla\cdot\mathbf{E}_1) + \frac{\omega_1^2}{c^2}\mathbf{E}_1 &= -i\mu_0\omega_1(\mathbf{J}_{1L} + \mathbf{J}_{\rm NL})\\ \mathbf{J}_L &\cong \mathbf{E}_1\left(-\frac{i\varepsilon_0\omega_{\rm pe}^2}{\omega_{\rm ce}} + \frac{\varepsilon_0\omega_{\rm pe}^2\nu_e}{\omega_{\rm ce}^2}\right)\\ \mathbf{J}_{1\rm NL} &= -\frac{e}{2}\left(n^*\mathbf{v}_0 + n_0\mathbf{v}^*\right)\\ &= -\phi^*\phi_0(\mathbf{x}+i\mathbf{y})\frac{e\varepsilon_0}{m_e}\frac{k_0^3\omega_{\rm pe}^2}{2\omega^2\omega_{\rm ce}}.\end{aligned} \tag{16}$$

Substitution of (10) into (16) yields

$$\left[ik_{1z}\beta_D - D_1(\omega_1)\right]A_1 - iA_0F_1A^* = 0 \tag{17}$$

where A^* is the complex conjugate of the idler wave amplitude produced by mixing of the whistler and pump waves. The collisional damping and nonlinear production coefficients are

$$\beta_D = \frac{\nu_e\omega_1\omega_{\rm pe}^2}{2k_{1z}c^2\omega_{\rm ce}^2}\ \left(\mathrm{m}^{-1}\right), \quad F_1 = \omega_1\frac{e}{m_e}\frac{k_0^3\omega_{\rm pe}^2}{c^2 2\omega^2\omega_{\rm ce}}\ \left(\mathrm{V}^{-1}\mathrm{m}^{-3}\right). \tag{18}$$

The collisional damping is negligible in the topside of the ionosphere and β_D will be dropped when considering the whistler wave growth.

The idler wave is described by Poisson's equation with electron density fluctuations from the equation of continuity and velocity fluctuations from the equation of motion including the nonlinear ponderomotive force [4]. This gives the differential equation for the idler electric-field potential

$$\begin{aligned}\nabla^2\phi &= \frac{e}{\varepsilon_0}\left(n_e^L + n_e^{NL} - n_i^L\right), \quad n_e^L = \frac{\varepsilon_0}{e}k^2\chi_e\phi\\ n_i^L &= -\frac{\varepsilon_0}{e}k^2\chi_i\phi, \quad n_e^{NL} = \frac{i\varepsilon_0}{2m_e}\frac{\omega_{\rm pe}^2}{\omega}F_{\rm NL}\phi_0\mathbf{E}_1^*\cdot(\mathbf{x}-i\mathbf{y}).\end{aligned} \tag{19}$$

The electron and ion susceptibilities along with the ponderomotive force factor $F_{\rm NL}$ are

$$\begin{aligned}\chi_e &= \left(\frac{\omega_{\rm pe}^2}{\omega_{\rm ce}^2} - \frac{\omega_{\rm pe}^2k_z^2}{\omega^2k^2}\right), \quad \chi_i = -\frac{\omega_{\rm pi}^2}{\omega^2}\\ F_{\rm NL} &= \frac{k_x}{\omega_{\rm ce}}\left(\frac{k_{0x}^2}{\omega_{\rm ce}^2} - \frac{k_{0z}k_{1z}}{\omega_0\omega_1} - \frac{k_{1z}k_z}{\omega_1\omega} + \frac{k_{0z}k_z}{\omega_0\omega}\right)\end{aligned} \tag{20}$$

with a correction to the sign error in the original derivation for FNL given in [4]. Substitution of the scalar and vector fields from (10) gives the linearized equation

$$-k^2D(\omega)A - iFA_0A_1^* = 0,\ F = \frac{e\omega_{\rm pe}^2}{2m_e\omega}F_{\rm NL}\ \ \left(\mathrm{m}^{-1}\mathrm{V}^{-1}\right) \tag{21}$$

where the dispersion function $D(\omega)$ is for the LH wave. Note that the plasma environment for the idler potential $\phi(z)$ is

influenced by the ring velocity distribution through the pickup ion mass m_r in (11).

Combining (17) and (21) and neglecting the small collisional damping defined in (18) yield the nonlinear dispersion equation for the parametric conversion process

$$k^2 D(\omega) D_1^*(\omega_1) = |A_0|^2 F_1^* F \tag{22}$$

which approaches zero in the absence of a pump wave.

The temporal growth at a fixed location is accounted for by letting $\omega = \omega_r + \mathrm{i}\gamma$ and $\omega_1^* = \omega_{1r} + \mathrm{i}\gamma$ with a fixed pump at the real frequency ω_0. At resonance, the dispersion functions can be replaced by the linearized expressions $D(\omega) = i\gamma D'(\omega_r)$ and $D_1*(\omega) = i\gamma D_1'^*(\omega_{1r})$. Assuming that the electric field and electric potentials are uniform in space, the temporal growth rate [4] from (22) is

$$\begin{aligned} \gamma^2 &= \frac{-FF_1|A_0|^2}{k^2 D\prime(\omega_r) D_1'^*(\omega_{1r})} \\ &\cong \frac{|A_0|^2 c^2 F F_1 / \left(2\omega_{\mathrm{pe}}^2\right)}{k_z^2 \omega_{\mathrm{pe}}^2 + k^2\left[(1-\alpha)\omega_{\mathrm{pi}}^2 + \alpha\omega_{\mathrm{pr}}^2\right]} \\ \text{with} |A|^2 &= \frac{-F D_1'(\omega_{1r})}{F_1 k^2 D'^*(\omega_r)} |A_1|^2. \end{aligned} \tag{23}$$

When collisional damping is neglected, the derivatives in the dispersion equations are evaluated with equilibrium values obtained from the wave-matching analysis with $D(\omega) = 0$ and $D_1^*(\omega) = 0$. Equation (23) is the temporal growth solution for an absolute instability where the LH pump wave is generating whistler waves fixed point in space.

A stability analysis for whistler amplification involving energetic electron distributions [40], [41] can be applied to the ion-ring distribution described here. A stability criterion [42] is employed for the WTWPA analysis to determine whether a small perturbation will grow predominantly in space or time. The whistler waves may grow in time, at every point in space (absolute instability), or they may propagate away while growing in time (convective instability) by propagating through the plasma to arrive at quiescent point where amplification no longer occurs [9]. This distinction is important to the REDA analysis of the NC-13 data. If the instability is convective, it should be possible for propagating waves to be excited having real ω and complex k, that is, growing in space away from the source. If the instability is absolute, there will be growth from noise until the wave amplitude reaches a saturation level, but this is not observed. The existence of ω (k real) solutions with $\gamma > 0$ is a necessary and sufficient condition that the system be unstable, but further examination is necessary to determine whether the instability is convective or absolute. For the REDA model, an absolute instability would give rise to VLF broadband emissions not seen 500 km away, whereas convective instability would amplify whistlers passing through the active region.

A dispersion relation that relates wave a frequency ω and a spatial frequency k has some arbitrariness in analyzing the behavior of the propagating system [9]. Thus far, the whistler parametric system (17) and (21) has been viewed as temporal variations at a fixed location. The dispersive wave equations, however, can be interpreted as a spatially amplifying system that describes a convective instability. Spatial amplification uses a functional envelope A1 for the EM waves, which varies slowly in space compared to the $e^{ik_{1z}z}$ spatial structure as the wave passes through the activated plasma. The local spatial growth rate is found with $k_{1z} = k_{1zr} - i\beta_{1z} = k_{0z} - (k_{zr} - i\beta_z)$. When treated as an amplifying wave, solutions to (17) and (21) is grow spatially with the rate $\beta_z = -\beta_{1z}$ determined from

$$\begin{aligned} k_z &= k_{zr} - i\beta_z, \quad k_{1z}^* = k_{1zr} - i\beta_z \\ D(k_z) &= -i\beta_z D'(k_z),\ D_1^*(k_{1z}) = -i\beta_z D_1^{*\prime}(k_{1z}) \\ \text{giving } \beta_z^2 &= \frac{-FF_1|A_0|^2}{k^2 D'(k_z) D_1^{*\prime}(k_{1z})} = \frac{|A_0|^2 F F_1 k^2 \omega^2}{4k_{1z}k_z k_x^2 \omega_{\mathrm{pe}}^2} \\ \text{with } |A|^2 &= \frac{-F D_1'(k_{1z})}{F_1 k^2 D'^*(k_z)} |A_1|^2 = \frac{F k_{1z} k^2 \omega^2}{F_1 k_z k_x^2 \omega_{\mathrm{pe}}^2} |A_1|^2. \end{aligned} \tag{24}$$

The whistler mode may be an amplifying wave, which grows as it propagates through the active medium [28]. It can be established with the dispersion equation (22) that the WPA system is convective and can provide spatial amplification of whistler waves [42].

From (23) and (24), the temporal and spatial growth are related by geometric mean of the longitudinal group velocities for the whistler signal and LH pump waves

$$\frac{\gamma}{\beta_z} = \sqrt{\frac{D'(k_z) D_1'(k_{1z})}{D'(\omega_r) D_1'^*(\omega_{1r})}} = \sqrt{V_{gz} V_{1gz}} \tag{25}$$

and that the ratio of the magnitudes for idler and signal waves is independent of the pump wave magnitude.

A sampling of the growth rates for the LH pump wave whistler mode growing in time and space is summarized in Table II for the two experimental wave frequencies 300 Hz and 25.2 kHz and the two active plasma percentages $\alpha = 1\%$ and 10%. The local values of signal growth are proportional to the power $|A_0|^2$ of the LH pump, which varies along the propagation path.

TABLE II
TEMPORAL/SPATIAL GROWTH FOR THE SIMULATED WTWPA

Signal f_1	Plasma α	Pump γ_0	Signal γ	Signal β_z
300 Hz	0.01	1.81 x 10^3 s^{-1}	2.06 x 10^6 $\lvert A_0\rvert$ s^{-1}	1.60 $\lvert A_0\rvert$ m^{-1}
300 Hz	0.1	6.49 x 10^3 s^{-1}	1.51 x 10^7 $\lvert A_0\rvert$ s^{-1}	23.1 $\lvert A_0\rvert$ m^{-1}
25.2 kHz	0.01	2.43 x 10^3 s^{-1}	3.66 x 10^8 $\lvert A_0\rvert$ s^{-1}	222 $\lvert A_0\rvert$ m^{-1}
25.2 kHz	0.1	6.00 x 10^3 s^{-1}	3.71 x 10^8 $\lvert A_0\rvert$ s^{-1}	216 $\lvert A_0\rvert$ m^{-1}

This analysis thus far has only considered the eigenmodes of the whistler parametric system with the assumption that the pump amplitude is constant in both space and time. This uses the rocket exhaust as a generator, not an amplifier, of whistler mode waves. The wave generation solutions provide both an absolute instability with (24) and a convective instability with (25). The absolute instability process will incoherently generate a broad spectrum of whistler waves if there is no external control of the whistler frequency. Using the convective instability process can have the advantage of more efficient transfer of energy from a coherent source to provide control

of the propagation direction as the wave passes through the active pickup ion plasma.

The WTWPA needs a specification for whistler signal input and output. The input signal wave $\mathbf{E}_1$ with a frequency ω_1 will only extract energy from one portion of the pump field potential ϕ_0 at a single resonant frequency ω_0 determined from the matching conditions. The amplifier extracts energy from a narrow portion of the power spectrum of the pump at a resonant frequency that is dependent on the properties of the ambient plasma and the fraction of plasma in an activated state. For the whistler parametric amplifier, it is of interest to tap into as much as possible of the LH wave free energy source pump waves. The resonant solutions of (24) and (25) do not satisfy this requirement because for a whistler frequency ω_1 only the pump LH energy around frequency ω_0 can be employed. Use of the three plasma modes will deplete "holes" in the pump spectrum leaving the rest of the pump energy unused. Extracting energy from the entire spectrum of LH pump waves may employ scattering of the incident whistler modes into a wide spectrum of angles.

Consider conversion of the purely longitudinal ($k_{1x} = k_{1y} = 0$) whistler mode into an oblique whistler with a finite k_{1x}. This process is consistent with the NG-13 Cygnus burn data because the observed region of whistler amplification was spread through the well-known 19.5° energy cone around the earth's magnetic field [28], [39]. Wave matching shows the production of an idler wave with a field-aligned whistler and a finite k_{0z} LH pump (i.e., Fig. 15). This LH idler wave can mix with a different pump wave oscillation to produce a whistler in another oblique direction. Thus, resonant scattering can broaden the directional spectrum of the whistler waves that leave the REDA region having extracted energy from a wider range of pump frequencies.

Exponential temporal or spatial growth, as $e^{\gamma t}$ or $e^{\beta z z}$, will eventually saturate the amplifier. At this point, the wave energy would approach the amount of energy going into the wave from the pump wave source. The point in the propagation where amplifier saturates and the pump starts to be depleted is found by considering the energy flux and the stored energy in the WPA system. Pump depletion is a critical factor required to determine the maximum amount of kinetic energy from the rocket exhaust and pump LH waves that can be converted into useful whistler mode energy.

III. Pump Depletion and Signal Propagation

Energy conservation provides a basis for determining the maximum output power of the WTWPA. Thus far, the REDA theory has covered all of the elements in the WPA system diagram illustrated in Figs. 2 and 12, which assumes that the amplified whistler and generated idler waves have much less energy than the pump. This is the small signal approximation. The source kinetic energy is converted into electrostatic wave energy with an efficient coefficient α_S defined in (3). The LH wave energy available for amplification of a whistler signal at frequency ω_1 is restricted to a wave frequency region at ω_0 and some of the pump energy is transferred to the idler wave ω. The electrostatic energy [28] in the LH pump and idler waves at each location z is given as

$$W_{\mathrm{ES}}(z) = \frac{\varepsilon_0|A_0(z)|^2}{4}F_{\mathrm{ES0}}(k_{0x}, k_{0z}, \omega_0) + \frac{\varepsilon_0|A(z)|^2}{4}F_{\mathrm{ES}}(k_x, k_z, \omega)$$
$$\text{where } F_{\mathrm{ES}}(k_x, k_z, \omega) = k_x^2\left(1 + \frac{\omega_{\mathrm{pi}}^2}{\omega^2} + \frac{\omega_{\mathrm{pe}}^2}{\omega_{\mathrm{ce}}^2}\right) + k_z^2\left(\frac{\omega_{\mathrm{pe}}^2}{\omega^2}\right). \tag{26}$$

The WPA energy comes from the pump wave with an energy distribution given by $W_{0S} = \varepsilon_0|A_{0S}(z)|^2F_{\mathrm{ES0}}/4 = \alpha_S W_{rS}$. Energy conservation requires that the total energy into the WPA system is equal to sum of the internal energies. Neglecting any energy absorbed as the whistler passes through the activated plasma media, the total electrostatic energy is

$$W_T = \frac{\varepsilon_0|A_{0S}(z)|^2}{4}F_{\mathrm{ES0}} = \frac{\varepsilon_0|A_0(z)|^2}{4}F_{\mathrm{ES0}} + \frac{\varepsilon_0|A(z)|^2}{4}F_{\mathrm{ES}}. \tag{27}$$

Solving for the WTWPA driving potential at each location along the amplifier path gives

$$|A_0(z)|^2 = |A_{0S}(z)|^2 - \frac{F_{\mathrm{ES}}}{F_{\mathrm{ES0}}}|A(z)|^2 = |A_{0S}(z)|^2 + \frac{F_{\mathrm{ES}}}{F_{\mathrm{ES0}}}\frac{FD_1'(k_{1z})}{F_1k^2D'^*(k_z)}|A_1|^2 \tag{28}$$

where the idler potential amplitude is related to the signal amplitude by the last equation in (24). Equation (28) represents pump depletion because $D'^*(k_z) < 0$ and the electrostatic pump wave transferring electrostatic energy to the idler wave. This underestimates pump depletion by ignoring energy transferred to the whistler wave. The limiting saturation effects of strong whistler amplification are seen in the spatial growth given by β_z in (24) with the pump amplitude given by (28).

The EM Poynting flux represents the transport of energy through the amplifier with a medium having negative ac conductivity. The WPA equations for propagation along B through the ring-beam plasma can be obtained by using the Poynting theorem for energy conservation [28]. Time averaging over a cycle yields the conservation law for the real Poynting vector

$$\nabla\cdot\mathbf{S} = -\frac{1}{2}\mathrm{Re}\left(\mathbf{E}_1\cdot\mathbf{J}_L^* + \mathbf{E}_1\cdot\mathbf{J}_{\mathrm{NL}}^*\right)$$
$$\text{with } \mathbf{S} = \frac{1}{2}\mathrm{Re}\left(\mathbf{E}_1\times\mathbf{H}_1^*\right) = \frac{1}{2}\mathrm{Re}\left(\frac{\mathbf{E}_1\times\mathbf{B}_1^*}{\mu_0}\right) = \frac{k_{1z}A_1(z)^2}{\mu_0\omega_1}\mathbf{z}. \tag{29}$$

The linear and nonlinear currents are given in (16) as

$$\mathbf{J}_{1L}^* \cong \mathbf{E}_1^*\left(\frac{i\varepsilon_0\omega_{\mathrm{pe}}^2}{\omega_{\mathrm{ce}}} + \sigma_D\right) \text{ with } \sigma_D = \frac{\varepsilon_0\omega_{\mathrm{pe}}^2\nu_e}{\omega_{\mathrm{ce}}^2}$$
$$\mathbf{J}_{\mathrm{NL}}^* = -\phi^*\phi_0(\mathbf{x} - i\mathbf{y})\frac{F_1}{\mu_0\omega_1} \equiv \sigma_{\mathrm{NL}}\mathbf{E}_1^*. \tag{30}$$

The collisional positive conductivity of the plasma gas, σ_D, provides damping of the whistler wave. The nonlinear negative conductivity, σ_{NL}, defined for the activated plasma at the

TABLE III
CONDUCTIVITY AND IDLER-TO-SIGNAL FRACTION FOR THE WTWPA

Signal f_1	Plasma α	σ_D (Siemans)	σ_{NL} (Siemans)	$\lvert A\rvert^2/\lvert A_1\rvert^2$
300 Hz	0.01	0.00148	-1.414 $\lvert A_0\rvert$	0.00588
300 Hz	0.1	0.000148	-20.725 $\lvert A_0\rvert$	0.0456
25.2 kHz	0.01	1.77×10^{-6}	-20.830 $\lvert A_0\rvert$	0.000180
25.2 kHz	0.1	1.77×10^{-6}	-21.227 $\lvert A_0\rvert$	0.000179

whistler frequency, provides growth of the wave. Substitution of (24) into (30) gives

$$\sigma_{\rm NL} = -\frac{|A_0|A}{A_1}\frac{F_1}{\mu_0\omega_1} = -\frac{|A_0(z)|}{\mu_0\omega_{\rm pe}}\frac{k\omega}{k_x\omega_1}\sqrt{FF_1\frac{k_{1z}}{k_z}} < 0 \quad (31)$$

yielding a negative conductivity that represents the wave growth. Negative conductivity is a common feature of microwave parametric amplifiers [43]. With these conductivities, (29) becomes

$$A_1'(z) + \frac{\mu_0\omega_1}{2k_{1z}}[\sigma_D + \sigma_{\rm NL}(z)]A_1(z) = A_1'(z) + \big[\beta_D - \beta_z(z)\big]A_1(z) = 0 \quad (32)$$

where the damping rate is from (18) and the growth rate is from (24). Equation (32) provides a convenient way to compute signal amplification including the effects of pump depletion using (28).

The computed conductivities and idler to signal amplitude ratios for the examples from Table II, and represented for $\alpha = 0.1$ by Figs. 13 and 14, are given in Table III. All of the nonlinear conductivities are negative and proportional to the pump wave amplitude given by the depletion-limited formula (28). The threshold for REDA gain occurs when the LH pump A_0 is large enough to make the total plasma conductivity $\sigma_T = \sigma_D - \sigma_{\rm NL}$ less than zero. The magnitude of the idler electric field is always less than that of the whistler signal wave.

The plasma WPA is a TWPA which has similarities to microwave TWPA designs based on materials containing Josephson junctions [44], [45]. Just like the whistler parametric amplifier, pump power in the Josephson TWPA (JTWPA) is converted into the signal and the idler and they have large gains per unit length. This results in pump depletion that leads to reduction of the signal gain and, finally, to gain saturation. This effect dramatically limits the amplifier dynamic range [44], [46], [47]. All of these effects are also found in the WTWPA.

The effects of pump depletion and resulting amplifier saturation can be demonstrated for the WTWPA by solving (32) with the negative plasma conductance given by (31). The depletion-limited pump is represented by (28) with the exhaust-driven LH waves of the form

$$A_{0S}(z) = A_{0M}\cos\left(\frac{\pi}{2}\frac{z}{z_{\rm SM}}\right)^2 \quad \text{for} -z_{\rm SM} \le z \le z_{\rm SM} \quad (33)$$

which is consistent with the activated-ion-region shape in Fig. 4. The pump-source electric field, $E_{0S} = A_{0S}(z)k_0$, is the dashed line in Figs. 16 and 17.

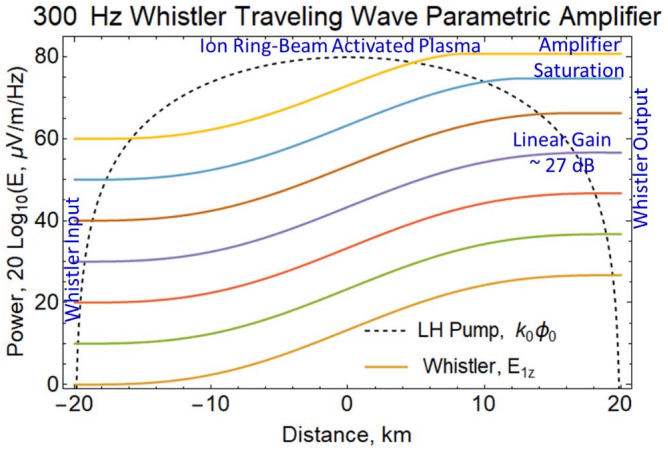

Fig. 16. Wide dynamic range for 300-Hz signals passing through the WTWPA. Maximum pump potential $A_{0M} = 100$ μV. The whistlers are amplified by about 27 dB after passing through 40 km of the REDA activated plasma.

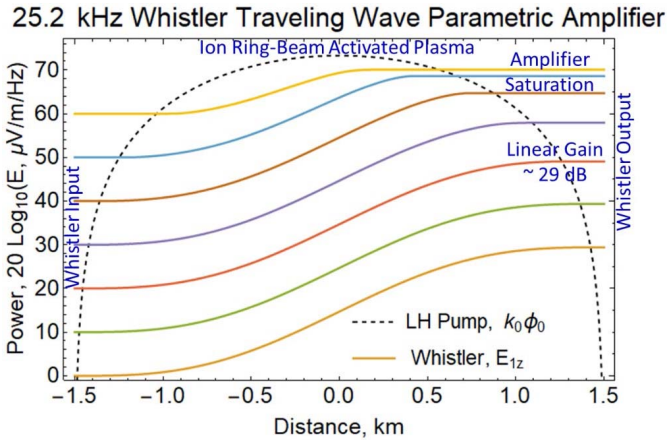

Fig. 17. Amplification of a 25.2-kHz signal with whistler wavelength $\lambda_1 = 655$ m by LH pump with wavelength $\lambda_0 = 0.14$ m and maximum potential $A_{0M} = 10$ μV. The whistlers are amplified by about 29 dB after passing through 3 km of the REDA activated plasma. Higher-amplitude whistler waves will eventually saturate as they propagate through the region of activated plasma.

The first illustration of the WTWPA is for a 300-Hz signal traveling through 42 km of an ion-ring beam plasma. The amplifier conditions are defined by the first two rows of Tables II and III. The LH pump potential is set to 100 μV to give a linear amplifier gain of 27 dB (Fig. 16). The whistler wavelength is 6.0 km and the LH pump wavelength is 0.64 m in the plasma. Saturation begins only when the input signal electric field goes above 40 dB(μV/m/Hz).

When the 25.2-kHz whistler signal passes through the activated plasma represented by last two rows in Tables II and III, plasma cloud dimensions has to be reduced to 3 km and the pump wave amplitude has to be reduced to 10 mV to give a linear gain of 29 dB. The whistler amplitude of the signal monotonically increases as illustrated with the solid curves in Fig. 17. The WTPWA shows a 40-dB linear dynamic range over an input signals above 0 dB (μV/Hz) before gain compression starts. Input signals above 40 dB (μV/Hz) are driven into saturation. The enhanced gain at higher frequencies is consistent frequency dependence of β_z in Table II.

Validation of the WTWPA theory should be explored with future REDA experiments. Frequency and power stepping of ground VLF transmitters could be used to determine the efficiency, linearity, and saturation levels of the amplification process. The 300-Hz WTWPA requires a 100 μV pump wave at 6.751 kHz that has an internal energy of 2×10^{-16} J. The 25.2 kHz requires only 10-μV LH pump potential with an internal energy of 7.2×10^{-18} J. The conversion efficiencies for a neutral jet to excite the LH pump wave α_S in (3) are 8×10^{-7} and 3×10^{-8}, respectively, for the 300-Hz and 25.2-kHz whistler signals. Thus, only a small amount of the exhaust kinetic energy is needed to provide substantial amplification of a whistler waves in space. The LH pump amplitude for Fig. 17 was chosen to produce a WTWPA gain similar to the observations shown in Fig. 1.

IV. Conclusion

A WTWPA has been developed using second-order nonlinear plasma theory to explain strong REDA [1]. During the NG-13 flight of Cygnus, BT-4 rocket engine burn demonstrated that kinetic energy from a hypersonic neutral jet could be transferred to whistler waves in a space plasma. The WTWPA employs charge exchange of rocket exhaust injected perpendicular to the earth's magnetic field to drive LH waves that act as an electrostatic pump for a plasma parametric amplifier. An external whistler wave is the input signal for the parametric amplifier and a second LH wave is the idler signal that satisfies the necessary conditions for frequency and wavenumber matching. The nonlinear ponderomotive force from electron momentum and the nonlinear currents that drive the whistler wave equation provide second-order nonlinearities in the WTWPA. Spatial growth is established as the whistler propagates though an activated plasma medium, which has a negative conductivity at the matched wave frequency ω_1. Negative conductance has long been known for microwave parametric amplifiers [43], but not for plasma devices. The whistler wave and idler wave grows exponentially when passing through this medium until either the signal leaves the active region or the LH pump wave is depleted by transferring electrostatic energy to the idler and signal waves.

The WTWPA model provides a useful description of broadband whistler wave amplification that is powered by rocket exhaust plume injected across magnetic field lines. The broadband feature is a result of the broad spectrum of LH waves excited by the energetic ion-ring distribution of gyrating pickup ions. This broadband nature implies that only a small fraction of the available LH wave energy is extracted to amplify a specific narrowband whistler signal. The conversion of chemical energy into amplified EM energy has low efficiency based on both the WTWPA model and on measurements during the Cygnus NG-13 experiment [1]. The efficiency estimates range from $\alpha_S = 4.8 \times 10^{-6}$ for amplification along a whistler ray path to $\alpha_S = 2.4 \times 10^{-4}$ for amplification and scattering into the 19° propagation cone for the whistler mode [1]. There is, however, an abundance of kinetic energy from the chemical reactions producing rocket plume and both experiment and models demonstrate that the gain of the WTWPA can easily be greater than 30 dB for a typical exhaust cloud from a small, 150 g/s, hydrazine rocket engine.

There are several improvements and extensions needed to complete the WTWPA model. The exhaust plume and conversion to an ion-ring distribution by charge exchange has not been quantitatively represented. A direct-simulation Monte-Carlo (DSMC) for rarefied space environments [48] coupled to a momentum and charge-exchange particle-in-cell (MPIC) kinetic model [49] could provide the evolution of the ring velocity distribution. The pump fields are oblique LH waves, which are established with maximum growth based on linear theory of the LH instability. The amplitudes and frequency spectrum of pump and the impact of pump depletion need to be estimated with an electrostatic (PIC) simulation coupled to an EM model for the propagating whistler wave. The whistler mode may be treated with fluid electrons and Maxwell's equations of EM fields that interact with the electrostatic fields of the pump and idler waves.

Future experiments in space and in the laboratory should be conducted to validate the theory developed in this article. Every five to seven months, a Cygnus satellite is launched into low-earth-orbit with a primary mission to service the International Space Station (ISS). After finishing the primary mission, Cygnus undocks from the ISS and is available for secondary missions such as demonstrating the REDA. Future experiments with dedicated Cygnus burns over ground VLF transmitters are planned. Finally, the REDA device illustrated in Fig. 2 could be set up in the laboratory as a large plasma device with an axial plasma column aligned with a cylindrical magnetic field. Experiments with this device could validate the presence of the three waves involved in the parametric amplification process.

Acknowledgment

The author would like to thank Dr. D. Winske, Dr. V. Sotnikov, and Dr. W. Scales for the theoretical discussions.

References

[1] P. A. Bernhardt *et al.*, "Strong amplification of ELF/VLF signals in space using neutral gas injections from a satellite rocket engine," *Radio Sci.*, vol. 56, no. 2, Feb. 2021, Art. no. e2020RS007207, doi: 10.1029/2020rs007207.

[2] E. Eliasson and K. Papadopoulos, "Numerical study of mode conversion between lower hybrid and whistler waves on short-scale density striations," *J. Geophys. Res.*, vol. 113, Sep. 2008, Art. no. A09315.

[3] E. E. Camporeale and G. L. P. D. olestock, "Lower hybrid to whistler mode conversion on a density striation," *J. Geophys. Res.*, vol. 117, Oct. 2012, Art. no. A10315.

[4] P. Kumar and V. K. Tripathi, "Parametric conversion of a lower hybrid wave into a whistler in a plasma," *Phys. Plasmas*, vol. 15, May 2008, Art. no. 052107.

[5] M. K. Saxena, "Decay of the lower-hybrid wave into an ion cyclotron mode and a whistler wave," *J. Plasma Phys.*, vol. 28, pp. 149–157, Aug. 1982.

[6] R. Bharuthram and M. Y. Yu, "Whistler wave generation by parametric decay of fast ion-acoustic waves," *Astrophys. Space Sci.*, vol. 146, no. 2, pp. 355–360, 1988.

[7] S. P. Kuo and R. J. Barker, "Parametric excitation of whistler waves by circularly polarized electromagnetic pumps in a nonuniform magnetoplasma: Modeling and analysis," in *Directions in Electromagnetic Wave Modeling*, H. L. Bertoni and L. B. Felsen, Eds. Boston, MA, USA: Springer, 1991.

[8] V. Sotnikov *et al.*, "Parametric excitation of very low frequency (VLF) electromagnetic whistler waves and interaction with energetic electrons in radiation belt," *Phys. Control. Fusion*, vol. 60, Mar. 2018, Art. no. 044014.
[9] P. A. Sturrock, "Kinematics of growing waves," *Phys. Rev.*, vol. 112, no. 5, pp. 1488–1503, Dec. 1958.
[10] L. Gomberoff and P. Vega, "Electrostatic instabilities driven by ion beams," *Plasma Phys. Control. Fusion*, vol. 32, p. 737, Sep. 1990.
[11] K. Akimoto, K. Papadopoulos, and D. Winske, "Lower-hybrid instabilities driven by an ion velocity ring," *J. Plasma Phys.*, vol. 34, no. 3, pp. 445–465, Dec. 1985.
[12] D. Winske and W. Daughton, "Generation of lower hybrid and whistler waves by an ion velocity-ring distribution," *Phys. Plasmas*, vol. 19, Jul. 2012, Art. no. 072109.
[13] S. Rosenberg and W. Gekelman, "A three-dimensional experimental study of lower hybrid wave interactions with field-aligned density depletions," *J. Geophys. Res., Space Phys.*, vol. 106, no. A12, pp. 28867–28884, Dec. 2001.
[14] A. Hasegawa and L. Chen, "Theory of plasma heating by nonlinear excitation of lower hybrid resonance," *Phys. Fluids*, vol. 18, pp. 1321–1326, Oct. 1975.
[15] V. K. Tripathi, C. Grebogi, and C. S. Liu, "Unified formalism of lower hybrid parametric instabilities in plasmas," *Phys. Fluids*, vol. 20, no. 9, p. 1525, 1977.
[16] G. Ganguli, L. Rudakov, W. Scales, J. Wang, and M. Mithaiwala, "Three dimensional character of whistler turbulence," *Phys. Plasmas*, vol. 17, no. 5, May 2010, Art. no. 052310.
[17] P. A. Bernhardt, "A critical comparison of ionospheric depletions chemicals," *J. Geophys. Res.*, vol. 92, no. A5, pp. 4617–4628, 1987.
[18] P. A. Bernhardt *et al.*, "Satellite observations of strong plasma wave emissions with frequency shifts induced by an engine burn from the cygnus spacecraft," *Radio Sci.*, vol. 56, no. 2, Feb. 2021, Art. no. e2020RS007143.
[19] P. A. Bernhardt and M. P. Sulzer, "Incoherent scatter measurements of ring-ion beam distributions produced by space shuttle exhaust injections into the ionosphere," *J. Geophys. Res., Space Phys.*, vol. 109, no. A2, Feb. 2004, Art. no. A02303.
[20] P. A. Bernhardt *et al.*, "Ground and space-based measurement of rocket engine burns in the ionosphere," *IEEE Trans. Plasma Sci.*, vol. 40, no. 5, pp. 1267–1286, Mar. 2012.
[21] T. Okumura *et al.*, "Observation of electron density depletion due to maneuver operation of H–II transfer vehicle," *J. Geophys. Res., Space Phys.*, vol. 124, no. 3, pp. 2238–2255, Mar. 2019.
[22] J. B. Hsia, S. M. Chiu, M. F. Hsia, R. L. Chou, and C. S. Wu, "Generalized lower-hybrid-drift instability," *Phys. Fluids*, vol. 22, pp. 1737–1746, Sep. 1979.
[23] R. L. Berger and F. W. Perkins, "Thresholds of parametric instabilities near the lower-hybrid frequency," *Phys. Fluids*, vol. 19, no. 3, p. 406, 1976.
[24] D. Riggin and M. C. Kelley, "The possible production of lower hybrid parametric instabilities by VLF ground transmitters and by natural emissions," *J. Geophys. Res.*, vol. 87, pp. 2545–2548, Apr. 1982.
[25] M. Mithaiwala, L. Rudakov, and G. Ganguli, "Stability of an ion-ring distribution in a multi-ion component plasma," *Phys. Plasmas*, vol. 17, no. 4, Apr. 2010, Art. no. 042113.
[26] M. Mithaiwala, L. Rudakov, G. Ganguli, and C. Crabtree, "Weak turbulence theory of the nonlinear evolution of the ion ring distribution," *Phys. Plasmas*, vol. 18, no. 5, May 2011, Art. no. 055710.
[27] W. A. Scales, G. Ganguli, L. Rudakov, and M. Mithaiwala, "Model for nonlinear evolution of localized ion ring beam in magnetoplasma," *Phys. Plasmas*, vol. 19, no. 6, Jun. 2012, Art. no. 062902.
[28] D. G. Swanson, *Plasma Waves*. Boston, MA, USA: Academic, 1989, pp. 75–173.
[29] A. Zhao and Z. Gao, "Convective amplification of a three-wave parametric instability in inhomogeneous plasma," *Phys. Plasmas*, vol. 20, no. 11, Nov. 2013, Art. no. 114503.
[30] M. N. Rosenbluth, "Parametric instabilities in inhomogeneous media," *Phys. Rev. Lett.*, vol. 29, p. 565, Aug. 1972.
[31] G. R. Mitchel, T. W. Johnston, and B. Grek, "Convective Brillouin amplification in drifting plasmas," *Phys. Fluids*, vol. 25, no. 1, p. 186, 1982.
[32] N. A. M. L. Khateeb and A. Nabil, "Convective amplification of stimulated Raman backscattering in inhomogeneous plasmas," *Arabian J. Sci. Eng.*, vol. 19, p. 175, Apr. 1994.
[33] G. New, *Introduction to Nonlinear Optics*. Cambridge, U.K.: Cambridge Univ. Press, 2011, pp. 23–24.
[34] J. M. Manley and H. E. Rowe, "Some general properties of nonlinear elements—Part I," *Proc. IRE*, vol. 44, no. 7, pp. 904–913, Jul. 1956.
[35] R. A. Martin and H. Segur, "Toward a general solution of the three-wave partial differential equations," *Stud. Appl. Math.*, vol. 137, no. 1, pp. 70–92, Jul. 2016.
[36] J. J. Angerami, "Whistler duct properties deduced from VLF observations made with the OGO 3 satellite near the magnetic equator," *J. Geophys. Res.*, vol. 75, no. 31, pp. 6115–6135, Nov. 1970.
[37] U. Motschmann, K. Sauer, and K. Baumgaertel, "Whistler wave amplitude oscillation and frequency modulation in the magnetospheric cavity," *Astrophys. Space Sci.*, vol. 105, no. 2, pp. 373–377, 1984.
[38] D. R. Nicholson, *Introduction to Plasma Theory*. New York, NY, USA: Wiley, 1983, pp. 177–185.
[39] K. S. Yeh and C. H. Liu, *Theory of Ionospheric Waves*. New York, NY, USA: Academic, 1972, p. 192.
[40] J. C. Lee and F. W. Crawford, "Stability analysis of whistler amplification," *J. Geophys. Res.*, vol. 75, no. 1, pp. 85–96, Jan. 1970.
[41] K. B. Dysthe, "Some studies of triggered whistler emissions," *J. Geophys. Res.*, vol. 76, no. 28, pp. 6915–6931, Oct. 1971.
[42] H. Derfler, "Growing wave and instability criteria for hot plasmas," *Phys. Lett. A*, vol. 24, no. 13, pp. 763–764, Jun. 1967.
[43] M. Uenohara, *Low Noise Amplification, Handbuch der Physik*, vol. 23. Berlin, Germany: Springer, 1962.
[44] A. B. Zorin, "Flux-driven Josephson traveling-wave parametric amplifier," *Phys. Rev. A, Gen. Phys.*, vol. 12, no. 4, Oct. 2019, Art. no. 044051.
[45] A. Miano and O. A. Mukhanov, "Symmetric traveling wave parametric amplifier," *IEEE Trans. Appl. Supercond.*, vol. 29, no. 5, pp. 1–6, Aug. 2019.
[46] K. O'Brien, C. Macklin, I. Siddiqi, and X. Zhang, "Resonant, phase matching of Josephson junction traveling wave parametric amplifiers," *Phys. Rev. Lett.*, vol. 113, Oct. 2014, Art. no. 157001.
[47] A. B. Zorin, "Flux-driven josephson traveling-wave parametric amplifier," *Phys. Rev. A, Gen. Phys.*, vol. 12, no. 4, Oct. 2019, Art. no. 044051.
[48] C. R. Kaplan and P. A. Bernhardt, "Effect of an altitude-dependent background atmosphere on shuttle plumes," *J. Spacecraft Rockets*, vol. 47, pp. 700–703, Jul. 2010.
[49] P. N. Giuliano and I. D. Boyd, "Effects of detailed charge exchange interactions in DSMC-PIC simulation of a simplified plasma test cell," in *Proc. 32nd Int. Electr. Propuls. Conf. (IEPC)*, 2011, pp. 1–10.

Paul A. Bernhardt (Fellow, IEEE) received the B.S. degree from the University of California at Santa Barbara, Santa Barbara, CA, USA, in 1971, and the M.S. and Ph.D. degrees from Stanford University, Stanford, CA, USA, in 1972 and 1976, respectively, all in electrical engineering.

He has been a Principal Investigator on a number of NASA and DOD sponsored experiments. His theoretical research interests include modeling of nonlinear interactions of high-power radio waves in the ionosphere, numerical solutions of partial differential equations for fluids and waves, and reconstruction algorithms for tomographic imaging. He is currently the Head of the Space Use and Plasma Environment Research Section with the Plasma Physics Division, U.S. Naval Research Laboratory, Washington, DC, USA. He has authored over 165 articles in refereed journals. His current research interests include remote sensing of the upper atmosphere using radio techniques, including computerized ionospheric tomography, optical excitation by high power radio waves, and radar diagnostics space shuttle engine burns.

Dr. Bernhardt is a fellow of the American Physical Society. He was the Chairman for Commission H of the United States National Committee of the International Union of Radio Science from 1994 to 1997, and the Subcommission C4/D4 on Active Experiments of COSPAR Experiments from 1998 to 2004, a member and Books-Board Editor of the American Geophysical Union, and an Associate Editor of Radio Science. His awards and honors include the NSF CEDAR Prize Lecture in June 2010 and the E.O. Hulburt Annual Science Award at NRL in June 2012.